Acta Pharmaceutica Sinica B 2020;10(3):546–556

Chinese Pharmaceutical Association
Institute of Materia Medica, Chinese Academy of Medical Sciences

Acta Pharmaceutica Sinica B

www.elsevier.com/locate/apsb
www.sciencedirect.com

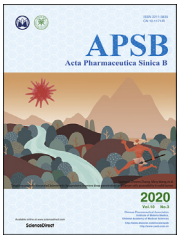

ORIGINAL ARTICLE

Reimaging biological barriers affecting distribution and extravasation of PEG/peptide-modified liposomes in xenograft SMMC7721 tumor

Hailing Tang[a,b,*], Mengjie Rui[c], Junhua Mai[d], Wei Guo[e], Yuhong Xu[b]

[a]*Institute of Molecular Medicine, Renji Hospital, Shanghai Jiao Tong University School of Medicine, Shanghai 200127, China*
[b]*School of Pharmacy, Shanghai Jiao Tong University, Shanghai 200240, China*
[c]*School of Pharmacy, Jiangsu University, Zhenjiang 212001, China*
[d]*Department of Nanomedicine, the Methodist Hospital Research Institute, Houston, TX 77030, USA*
[e]*Institute of Cancer Stem Cell, Dalian Medical University, Dalian 116044, China*

Received 10 April 2019; received in revised form 31 May 2019; accepted 17 June 2019

KEY WORDS

GE11;
Liposome;
Target delivery;
Biology barrier;
EGFR;
SMMC7721

Abstract Liposomes, as one of the most successful nanotherapeutics, have a major impact on many biomedical areas. In this study, we performed laser scanning confocal microscope (LSCM) and immunohistochemistry (IHC) assays to investigate the intra-tumor transport and antitumor mechanism of GE11 peptide-conjugated active targeting liposomes (GE11-TLs) in SMMC7721 xenograft model. According to classification of individual cell types in high resolution images, biodistribution of macrophages, tumor cells, cells with high epidermal growth factor receptor (EGFR) expression and interstitial matrix in tumor microenvironment, in addition, their impacts on intra-tumor penetration of GE11-TLs were estimated. Type I collagen fibers and macrophage flooded in the whole SMMC7721 tumor xenografts. Tumor angiogenesis was of great heterogeneity from the periphery to the center region. However, the receptor-binding site barriers were supposed to be the leading cause of poor penetration of GE11-TLs. We anticipate these images can give a deep reconsideration for rational design of target nanoparticles for overcoming biological barriers to drug delivery.

*Corresponding author. Tel.: +86 13564527091, +86 10 67061033.
E-mail address: hltang2010@163.com (Hailing Tang).

Peer review under responsibility of Institute of Materia Medica, Chinese Academy of Medical Sciences and Chinese Pharmaceutical Association.

https://doi.org/10.1016/j.apsb.2019.06.011

1. Introduction

Liposomes have been one of the most successful type of nanosize drug delivery systems in cancer therapy[1,2]. Doxil (liposomal doxorubicin[3,4]) and Onivyde (liposomal irinotecan)[5] are widely used in first line treatment of certain types of cancer in clinic. This inspired the development of various polymer or lipid-based nanoparticles[6,7]. Nano-delivery systems accumulate preferentially in tumor site due to the enhanced permeability and retention (EPR) effect[8,9]. However, enormous evidences[10−13] showed that conventional liposomes and nanoparticles might be easily sequestrated by mononuclear phagocyte system (MPS), and sequentially trapped in the lumen of vessels and the interstitial space of tumor, which limited the therapeutic efficiency of nanodrugs. Incorporation of poly(ethylene glycol) (PEG) to the surface of nanoparticles prolongs their circulating lifetimes[12,14−16]. Moreover, an "active stealth" approach was also explored by attaching "don't eat-me" marker CD47 "self" peptides to avoid phagocytic clearance[17,18].

Next generation liposome designs responding to the biological barriers have been proposed to optimize drug delivery and therapeutic efficacy. Multi-functional nanoparticles achieved the integration of diagnosis, imaging, active-targeting and triggered release properties[19,20]. To fully validate the achievements of such multi-potent system *in vivo*, it would be essential to develop methods to visualize the behavior of nanoparticles inside tumor tissues.

Epidermal growth factor receptor (EGFR) is frequently overexpressed in HCC and also a rational target for active targeting[21,22]. We previously reported a peptide, YHWYGYTPQNVI (GE11) which specifically and efficiently bound to EGFR high-expressing cancer cells *in vitro*. GE11-modified liposomal drugs also achieved extraordinary antitumor effect *in vivo*[23−25].

In this study, unmodified and GE11 peptide-modified PEGylated liposomes were used as model systems to investigate biological barriers affecting distribution and extravasation of liposomes in SMMC7721 HCC xenograft model. Histological analysis by laser scanning confocal microscope (LSCM) and immunohistochemistry (IHC) were used to investigate the cell subsets, their distribution patterns in tumor microenvironment and how they affected liposome penetration in tumors. Some strategies, such as co-administration of collagenase, were also implemented to identify the main determinants for GE11-TLs in SMMC7721 HCC xenografts, comparing to only PEGylated liposomes (PLs).

2. Materials and methods

2.1. Materials

Hydrogenated soybean phosphatidylcholine (HSPC) and 1,2-distearoyl-*sn*-glycero-3-phosphoethanolamine-*N*-[methoxy(polyethylene glycol)-2000](DSPE-PEG2000) were obtained from Japan NOF Corporation (Tokyo, Japan). Cholesterol was purchased from Avanti Polar Lipids (Alabaster, AL, USA). Rhodamine 1,2-dihexadecanoyl-*sn*-glycero-3-phosphoethanolamine (Rhodamine DHPE) were purchased from Invitrogen Corporation (Carlsbad, CA, USA). 1,2-Distearoyl-*sn*-glycero-3-phosphoethanolamine-*N*-[maleimide (polyethylene glycol)-2000] (ammonium salt) (DSPE-PEG2000-Mal) and GE11-cys (YHWYGYTPQNVIC) were synthesized by Pharmaron Inc. (Beijing, China) with a purity of 95% at least. The fluorescence dye 4,6-diamidino-2-phenylindole (DAPI) was from Roche (Sigma−Aldrich, St. Louis, MO, USA). Water was purified by a Millipore Milli-Q purification system (Millipore, Bedford, MA, USA). All other reagents were of chemical pure or analytical grade from Sinopharm Chemical Reagent Co., Ltd. (Shanghai, China).

2.2. Preparation of GE11/PEG-modified liposomes

To synthesize DSPE-PEG-2000-Mal-GE11, DSPE-PEG-2000-Mal and GE11-Cys were dissolved in 50 mmol/L HEPES buffer (pH 7.2, saturated with nitrogen) at a molar ratio of 1:2, and incubated overnight at 10 °C. The excess GE11-Cys and HEPES were removed with an Amicon ultra centrifugal filter device (Ultracel PL-1, Millipore). Conjugate efficient and purity of DSPE-PEG2000-Mal-GE11 were determined with a reverse phrase-high performance liquid chromatography (RP-HPLC) system (Agilent 1100, Agilent, Palo Alto, CA, USA) with an evaporative light scattering detector (ELSD) (SEDEX 75, SEDERE, Orléans, France).

Thin film method was used for preparation of GE11-conjugated rhodamine-labeled liposomes. Specifically, HSPC, CHOL, DSPE-PEG2000, DSPE-PEG2000-Mal-GE11 and (or) rhodamine DHPE were mixed in chloroform at fixed molar ratios, and dried into a thin film by a rotary evaporator. For PEG-modified liposomes (PLs), the lipid formulation is 6.54 μmol/mL HSPC, 3.0 μmol/mL CHOL, 0.40 μmol/mL DSPE-PEG2000, 0.06 μmol/mL rhodamine DHPE with the total lipid concentration of 10 μmol/mL. For GE11-modified liposomes (GE11-TLs), the lipid formulation is 6.4 μmol/mL HSPC, 2.94 μmol/mL CHOL, 0.40 μmol/mL DSPE-PEG2000 and 0.20 μmol/mL DSPE-PEG2000-GE11, 0.06 μmol/mL rhodamine DHPE with the total lipid concentration of 10 μmol/mL. The residual chloroform was removed by nitrogen stream. And then the lipid film was hydrated with phosphate buffered saline (PBS, pH 7.4), followed by sonication, and syringe extrusion. The size distribution and zeta potential of the liposomes were routinely tested using a Zeta-sizer Nano-zs90 (Malvern Instruments, Worcestershire, UK).

2.3. Xenograft animal models

Male nude mice (SLAC Company, Shanghai, China) at the age of 6−8 weeks were used in all studies. 2×10^6 SMMC7721 cells were resuspended in 100 μL of PBS and injected subcutaneously into the right flank of the mice to establish HCC xenograft models. When the tumors reached 100−200 mm^3, mice were sacrificed and tumors were collected and cut into 1 mm × 1 mm × 1 mm cubes. And then tumor cubes were implanted in the right flank of a new batch of nude mice. The animal model used in the research and the experiment protocols were approved by the animal study committee of School of Pharmacy, Shanghai Jiao Tong University (Shanghai, China).

2.4. Frozen section

Firstly, mice were i.v. administrated with 80 mg/kg PLs or GE11-TLs, combined with 30 mg/kg collagenase I or 16 mg/kg iRGD. After 1 h, mice were sacrificed and tumors were harvested for histological analysis. The xenografts were processed as follow: (1) samples were embedded in freezing medium OCT (Leika, Wetzlar, Germany); (2) freezed in liquid nitrogen for seconds; (3) placed in a freezing microtome (Leika CM1850, Leika, Wetzlar, Germany) until the tissue internal temperature balanced with

external condition; (4) blocks at a thickness of 14 μm were continuously cut; (5) the sections were fixed the at 4% paraformaldehyde for 15 min before immunostaining.

2.5. *Immunostaining*

Macrophage, tumor angiogenesis, EGFR, collagen I and collagen IV in SMMC7721 xenograft were labeled to investigate the biological barriers of HCC xenografts, as well as critical barrier factors affecting distribution and permeability of PEG/GE11-modified liposomes in tumor tissues. Briefly, rhodamine-labeled GE11-TLs or PLs at a lipid dose of 80 mg/kg were given *via* i.v. administration into SMMC 7721 tumor-bearing nude mice. To study the influence of collagenase type I on the distribution behavior of GE11-TLs, 30 mg/kg collagenase I was injected 1 h before liposomes administration. To study the impact of iRGD on permeability of GE11-TLs in tumor, iRGD was injected at a dose of 16 mg/kg 1 h before rhodamine-labeled liposomes adiministration. For immunostaining, the fixed tumor sections were washed with PBS for 3 times and then incubated with 5% donkey serum for 30 min at 37 °C. Then redundant donkey serum was sucked. Primary antibodies, rat anti-mouse CD105 against tumor neovascular (1:100 dilution, Ebioscience, San Diego, CA, USA), rat anti-mouse CD68 against macrophage (1:100 dilution, Ebioscience), rabbit anti-mouse collagen I (1:200 dilution, Abcom, Cambridge, UK), rabbit anti-mouse/human EGFR (1:200 dilution, Abcom), and rabbit anti-mouse collagen IV (1:200 dilution, Abcom) were dropped on the sections separately. Slides were then incubated at 4 °C overnight. After incubation, slides were washed with PBS 3 times, followed by staining with secondary antibody Alex488 donkey anti-rat IgG (1:200 dilution, Invitrogen, Carlsbad, CA, USA) for CD105 and CD68 or Alex488 donkey anti-rabbit IgG (1:200 dilution, Invitrogen) for collagen I, EGFR, collagen IV were added for observation of interstitial components of SMMC7721 by LSCM.

To co-localize EGFR and neovascular, collagen and neovascular, samples were stained with the same procedure above. The second antibody Dylight 549 donkey anti-rat IgG (1:200 dilution, Invitrogen) and Alex488 donkey anti-rabbit IgG were used to label the primary ones. Alexa Fluor® 633 WGA (Invitrogen) and DAPI (Sigma−Aldrich) were always used to stain the cellular membrane and nucleus at last.

To image the phagocytose rates of mononuclear cells, 200 μL rhodamine-labeled liposomes were given *via* tail vein at a 50 mg/kg lipid dose. Blood was taken at 6 and 12 h, respectively. Ficoll-hypaque solution was used to isolate mononuclear macrophage following the product manual. The third layer containing mononuclear macrophages was collected by centrifugation at 2800 rpm for 10 min (Centrifuge 5430, Eppendorf AG, Hamburg, Germany). After fixed with 1% paraformaldehyde, cell membrane was stained with Alexa Fluor® 633 WGA and nucleus was stained with DAPI for the observation of the binding and uptake of rhodamine-labeled liposomes by monocytes and erythrocytes.

2.6. *Laser scanning confocal microscope*

Distribution of rhodamine-labeled liposomes and localization of tumor angiogenesis, interstitial collagens (types I and IV), macrophage, and EGFR-expressed cells in SMMC7721 xenograft were studied using confocal laser scanning microscopy (Leica TCS SP8, Leica). Co-localization of EGFR and blood vessels, collagen and blood vessels, rhodamine-labeled liposomes and blood vessels or collagen I were done using a 63/1.3 oil objective. Overview images were captured using a 40/1.3 oil objective. 405-nm Diode LASOS, 488-nm argon, 561-nm DPSS lasers were used to excite DAPI, Alexa Fluor 488, Rhodamine (or Dylight549 or Cy3.0), respectively. Distribution of fluorescence-labeled components per image was quantified by measuring fluorescence pixels to the entire tissue image pixels by histogram function of Photoshop CS4 software. Image merge and interstitial cell nucleus discoloration were processed by Image J combined with Photoshop CS4 software.

3. Results and discussion

3.1. *The characterization of interstitial cells in SMMC7721 xenografts*

To study the distribution of GE11-TLs in SMMC7721 xenografts, confocal microscope and IHC were employed to understand the pathophysiology of SMMC7721 tumor tissue by discriminating the cell subsets. The morphology of the hepatocellular cancer cell (SMMC7721) nuclei was visualized by DAPI staining (Fig. 1). SMMC7721 tumor cells were distinguished from normal hepatocytes *via* their nuclei with unique size, shape, margin and chromatin under high-resolution microscope (Fig. 1A−C). The normal hepatocyte nuclei are fully spherical shape with a diameter of approximately 10 μm, while the nuclei of SMMC7721 usually show variety of size, commonly known as pleomorphism, more than 10 μm in diameter. The nuclei pleomorphism makes it easy to discriminate SMMC7721 tumor cells from the interstitial cells. The nuclei of interstitial cells, such as macrophage, endothelial cell, pericyte, fibroblast, and myeloid derived suppressor cells (MSDC), are smaller with flatten or smaller normalized spherical form (Fig. 1C and D), comparing with those of SMMC7721 tumor cells. The SMMC7721 tumor cells always exhibited piles of growth (Fig. 1D), surrounding by loose and scattered interstitial cells. In order to know whether liposomes can penetrate from the blood vessels to the interstitial space, and eventually reach tumor cells, we decolorized the blue nuclei of interstitial cells in microscopic images to separate them from SMMC7721 cancer cells. As shown in Fig. 1E, the interstitial cells are heterogeneous from the periphery to the center through the entire tumor, mostly accumulated along the margin of tumor. These interstitial cells were always separated from the cluster of SMMC7721 by the over secretion of interstitial component, such as collagen fibers (Figs. 3A and 6). Before reaching the tumor cells, liposomes need to pass the interstitial space filling with interstitial matrix firstly, which forms the major barrier of liposome transport.

3.2. *The microenvironment characterization in SMMC7721 xenografts*

We used CD105, CD68, collagen I, collagen IV and EGFR antibodies to label tumor neoplastic epithelial cells, macrophage, interstitial matrix and the cells with EGFR expression, respectively, which are major components in tumor microenvironment, and may influence the distribution of GE11-TLs in tumor tissues (Figs. 2 and 3). Percentage of each component was calculated by dividing colored pixels to the entire tissue image pixels. As shown in Fig. 2, collagen I (Fig. 2C) is the most abundant interstitial matrix in SMMC7721 xenografts, which occupied

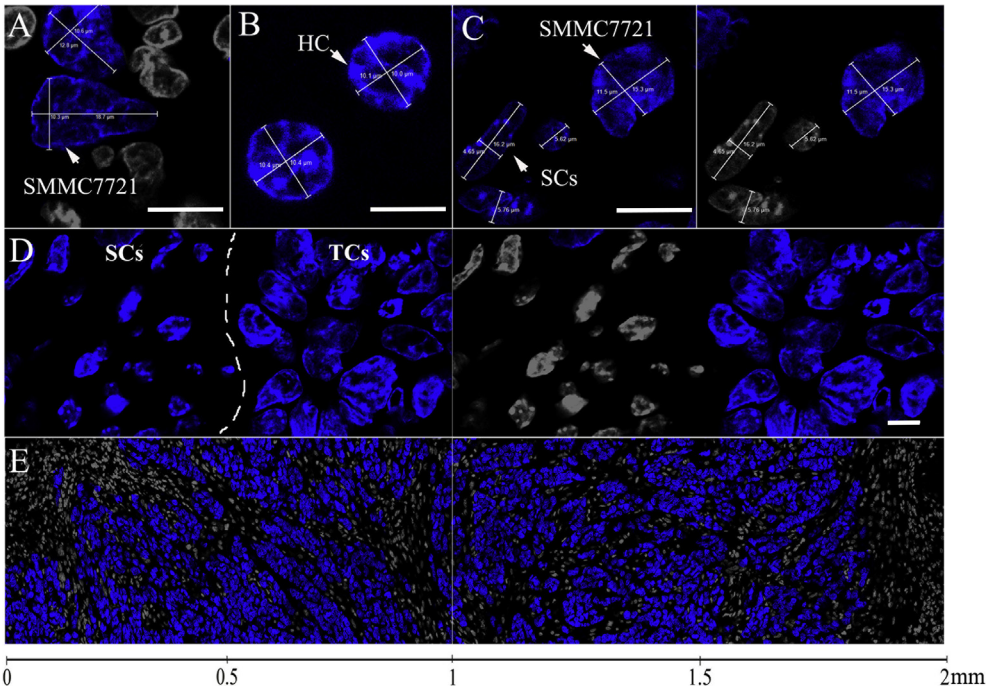

Figure 1 (A) The nucleus morphology of SMMC7721 tumor cells. (B) The nucleus morphology of hepatocytes (HC). (C) The nucleus morphology of SMMC7721 tumor cells *vs*. stromal cells in SMMC7721 xenografts (white: stromal cells; blue: SMMC7721 cell). Scale bar: 10 μm. (D) The patterns of clusters of SMMC7721 tumor cells and stromal cells (white: stromal cell; blue: SMMC7721 cell). Scale bar: 10 μm. (E) The detailed distribution of SMMC7721 tumor cells and stromal cells from the periphery to the center in SMMC7721 xenograft tumor (white: stromal cell; blue: SMMC7721 cell).

3.4% of the whole tissue size, followed by macrophage (1.8%, Fig. 2B), collagen IV (1.7%, Fig. 2A) and tumor neoplastic epithelial cells (1.2%, Fig. 2D). EGFR (Fig. 2E) was expressed not only in SMMC7721 cancer cells, but also in stromal cells. The tumor angiogenesis (Fig. 2D) was of great heterogeneity from the periphery to the center region in SMMC7721 xenografts. It existed mostly at the margin of tumor tissue, while sometimes appeared in the center where abundant interstitial cells separated the tumor tissue into several subunits for blood and nutrition supplies.

3.3. Distribution and extravasation determinants of GE11-TLs in SMMC7721 xenografts

The size distribution and zeta potential of the liposomes were routinely examined by photon correlation spectroscopy (PCS) using a Zeta-sizer Nano-zs90 (Malvern Instruments, UK). The size distribution is 119.9 ± 0.6 nm for PLs and 155.7 ± 4.1 nm for GE11-TLs, respectively. As for zeta potential, PLs is −2.9 ± 0.1 mV, GE11-TLs is −3.2 ± 0.6 mV.

Two rhodamine-labeled liposomes, GE11-TLs and PLs, were used to evaluate how the biological barriers affect GE11-TLs distribution in SMMC7721 xenografts. Only passive EPR effect contributes to the accumulation of PLs in tumor, whereas the active binding effect helps the accumulation of GE11-TLs as well (Fig. 4). Fig. 4 (A and B) presents the overall biodistribution patterns of rhodamine-labeled PLs (A), and GE11-TLs (B, PEG/GE11 = 4:2). After 1 h post i.v. injection, PLs and GE11-TLs occupied 2.3% and 13.1% of the entire tumor area (by fluorescence), respectively. The area of GE11-TLs was up to 6-fold higher than PLs, showing a fast accumulation and retention pattern at this time point. These images also indicated heterogeneity of distribution of liposomes in SMMC7721 xenografts. High fluorescence signal always localized in the peripheral area of xenografts and interstitial space abundant in blood vessels around tumor subunits (Fig. 4).

The accumulation of GE11-TLs was observed to exhibit higher specificity for the tumor neoplastic vasculature (Fig. 5B), comparing to PLs which give an observation of fluorescence spreading across the vessel and diffusing into interstitial area for several cell layers as shown in white discoloring area (Fig. 5A). But both of them were confined to the interstitial space and could not effectively reach the SMMC7721 cancer cell.

SMMC7721 xenograft was rich in collagen fibers (Figs. 2A, C and 3A). Recently, the use of collagenase for modulation of extracellular matrix (ECM) in tumors has succeeded in reducing interstitial fluid pressure (IFP) and improving the accumulation of liposomal doxorubicin in tumors[26–28]. The collagen I content is also likely the major determinant of interstitial transport for both GE11-TLs and PLs as shown in Figs. 2 and 6. Here, we used the maximum dose of collagenase-1 (30 mg/kg collagenase-1, while the lethal dose was 32 mg/kg) to study whether the collagenase could improve the distribution of two liposomal formulations in SMMC7721 HCC xenografts. After co-administration of collagenase I, increased fluorescence signal of PLs was observed obviously in the edge of tumor (Fig. 6A). However, the signal of GE11-TLs stayed the same (Fig. 6B). GE11-TLs only located around endothelial cells and did not extravasate further into the interstitial (Fig. 6C and D). But we still observed some slight changes of GE11-TLs, which exhibited even distribution throughout the whole xenografts after treatment of collagenase I. This may be due to the result of slight changes of blood flow that

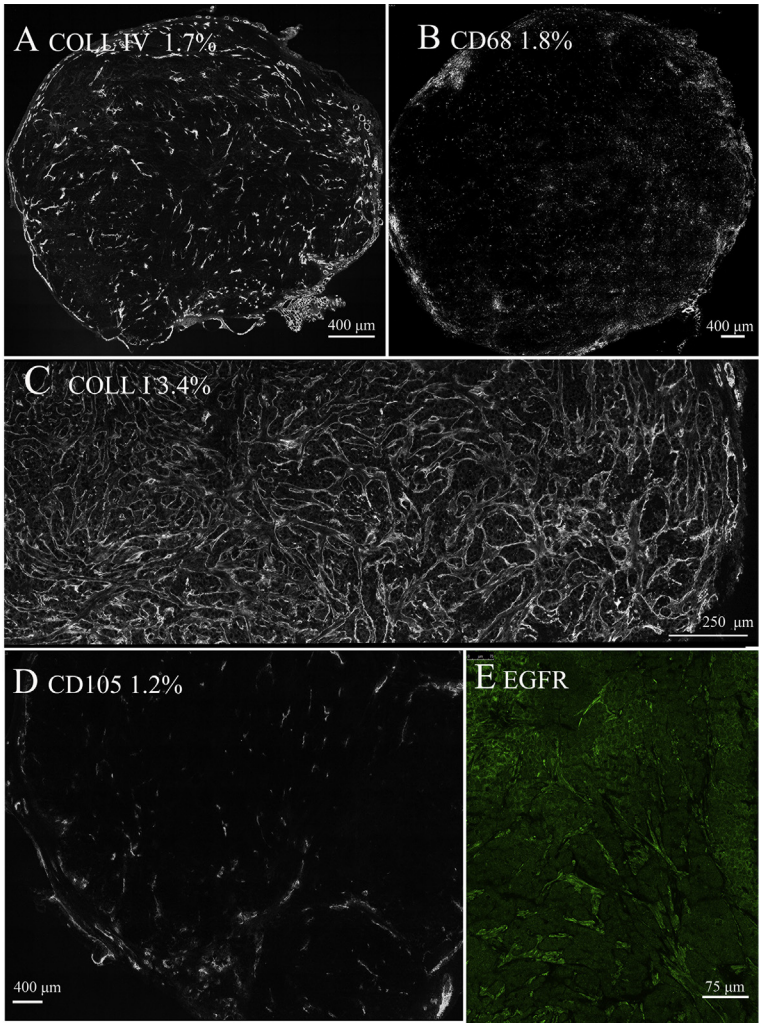

Figure 2 (A) The distribution of type IV collagen fibers in SMMC7721 xenograft. (B) The overview image of the distribution of CD68-labeled macrophage in SMMC7721 xenografts. (C) The distribution of type I collagen fibers in SMMC7721 xenografts. (D) The overview image of the distribution of CD105-labeled tumor angiogenesis in SMMC7721 xenografts. (E) The overview image of the distribution of EGFR in SMMC7721 xenografts.

benefits from the variation of trans-vascular pressure gradient and IFP. Both of the two formulations were still confined to interstitial space and could not successfully arrive at the tumor cell.

From these images, the maximum dose of collagenase did not dramatically degrade the collagen surrounding the tumor vessels and the cluster of SMMC7721 cells, when compared to untreated tumor ones. Collagen type I were existed in the whole tumor, although less abundant. However, it became sparser around vasculature from 1 h post treatment, which contributed to the deeper permeation of nanoparticles from tumor vessels into tumor stroma (Fig. 5).

Without collagenase I treatment, both GE11-TLs and PLs accumulated along the CD105 tumor neoplastic epithelial cells, where EPR effect occurred. Collagenase I improve the accumulation and diffusion of PLs at the new vessels in xenografts (Fig. 6A); however, GE11-TLs did not benefit from it (Fig. 6B) due to the abundant EGFR overexpressed in tumor tissues especially on interstitial cells, which constituted the site-binding barriers. We speculated that receptor-binding site barriers may be the major determinant of interstitial transport for ligand-mediated targeting liposomes, GE11-TLs, while the abundant collagen content may be the dominant one for PLs.

Due to the poor penetration of PLs and GE11-TLs in tumors, we attempted to employ a reported tumor-penetrating peptide, iRGD ((internalizing RGD, CRGDK/RGPD/EC) to promote vessel and tissue permeability in a tumor-specific and neuropilin-1-dependent manner[29,30]. We found that co-administration with iRGD peptide could not significantly improve permeability of the PLs and GE11-TLs in the SMMC7721 xenograft model (Figs. 7 and 8). Both PLs and GE11-TLs dispersed heterogenously in tumor. It is consistent with the Kandela et al. and Mantis et al.'s observation[31,32].

Though the tumor-associated macrophage labeled with CD68 spread widely in the whole tumor tissue (Figs. 2B and 9), it was not the pivotal barrier for the GE11-TLs due to the dysfunction of phagocytosis, when compared with the phagocytosis happened to the MPS in blood (Fig. 10).

Enormous papers were focused on the tumor growth inhibition and survival rate *in vivo* or tumor cell apoptosis caused by the active or passive targeting delivery vectors *in vitro*. But few

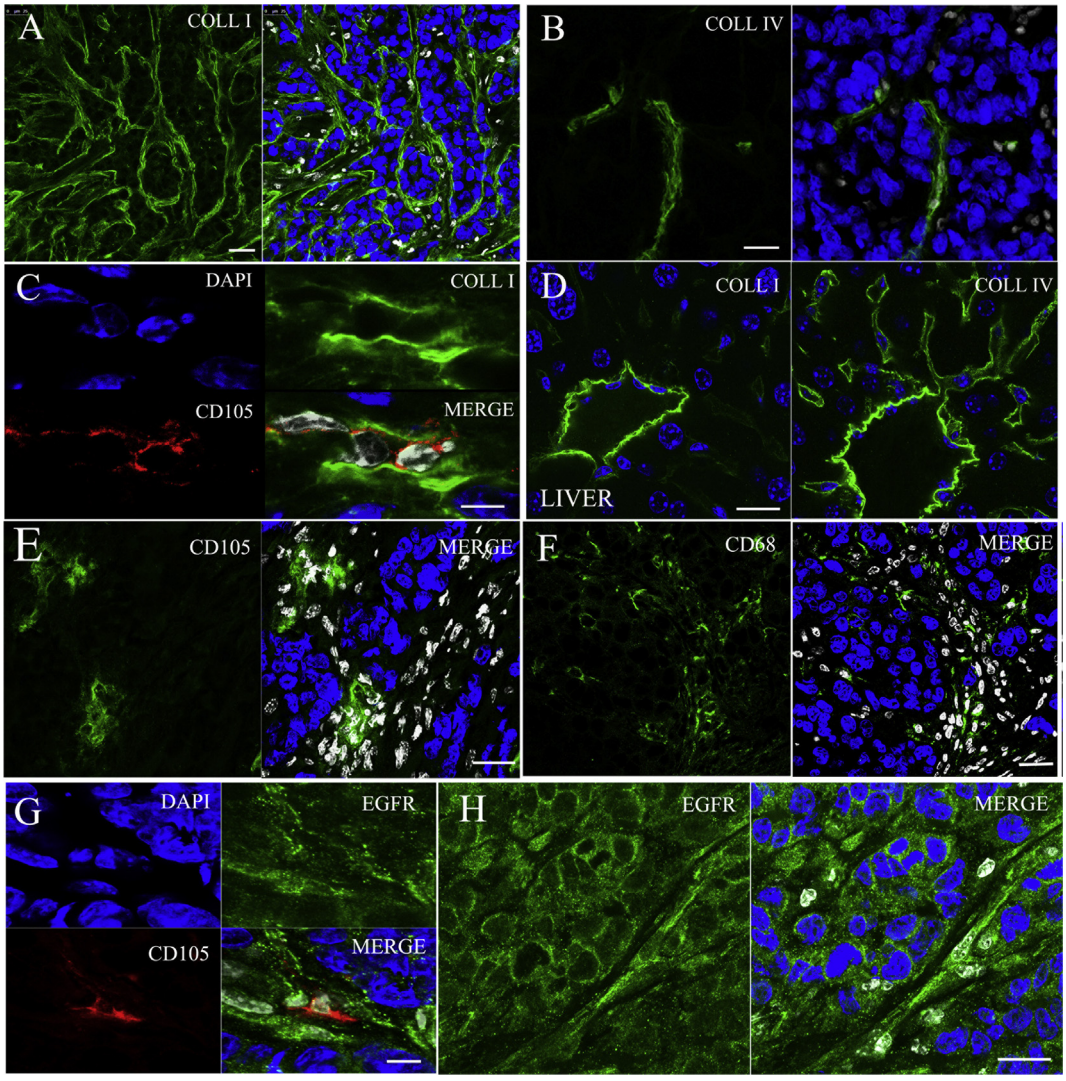

Figure 3 The detailed drawing of the distribution of type I collagen fibers (A) and type IV collagen fibers (B) in SMMC7721 xenograft tumor. Blue: nuclei; green: type IV or I collagen; white: stromal cells. Scale bar: 50 μm. (C) The detail drawing of CD105-labeled tumor angiogenesis distributed in collagen I-flooded SMMC7721 xenografts. Scale bar: 25 μm. (D) The detailed drawing of the distribution of type I and IV collagen fibers in normal liver tissue. Scale bar: 25 μm. (E) The detail drawing of CD105-labeled tumor angiogenesis, and (F) CD68-labeled macrophage distributed in SMMC7721 xenografts. Scale bar: 25 μm. (G) The expression of EGFR in the regions of tumor angiogenesis in SMMC7721 xenografts. Blue: nuclei; green: EGFR; red: CD105 to label the tumor neoplastic endothelial cell; white: stromal cell. Scale bar: 7.5 μm. (H) The detailed drawing of the distribution of EGFR in SMMC7721 xenograft. Blue: nuclei; green: EGFR; white: stromal cells. Scale bar: 25 μm.

data were focused on the detailed distribution of these targeting nano-DDS in the tumor site. In this study, images were captured to give clarity evidence. We found that SMMC7721 HCC xenografts was a kind of vascularized tumor with high heterogeneity and collagen I flooded in the whole xenografts surrounding both the cluster of SMMC7721 cells and vessels, while in normal liver tissues, collagen IV is the most abundant collagen matrix. Successful transport of GE11-TLs from the systemic circulation to SMMC7721 tumor cells acquired several processes. First, liposomes accumulate in tumor *via* neo-vessels. Second, they must cross the vessel wall to the interstitial space, and finally reach the target cell after overcoming the interstitial barriers.

From the images above, both rhodamine-labeled GE11-TLs and PLs were accumulated in neo-vasculature, and retarded in the neighboring region of tumor angiogenesis. Although PLs could spread across the vessel wall by diffusion, few of them overcame the interstitial barriers outside tumor clusters and reach tumor cells in reality, probably because of the high IFP and collagen content in tumor.

Even after collagenase and iRGD treatments decreased the elevated IFP and enhanced the permeability, increased accumulation of PLs occurred mainly on the margin of the tumor. Alternatively, for GE11-TLs, the binding site barriers were found to be leading obstacle, which limited the deeper penetration of GE-TLs. Also, administration of collagenase and iRGD barely affected GE11-TLs diffusion across the interstitial space. Collectively, the advantage of GE11 modification came from the higher retention and uptake of GE11-TLs by EGFR-expressed stroma cells adjoined to the endothelial cells, especially in the

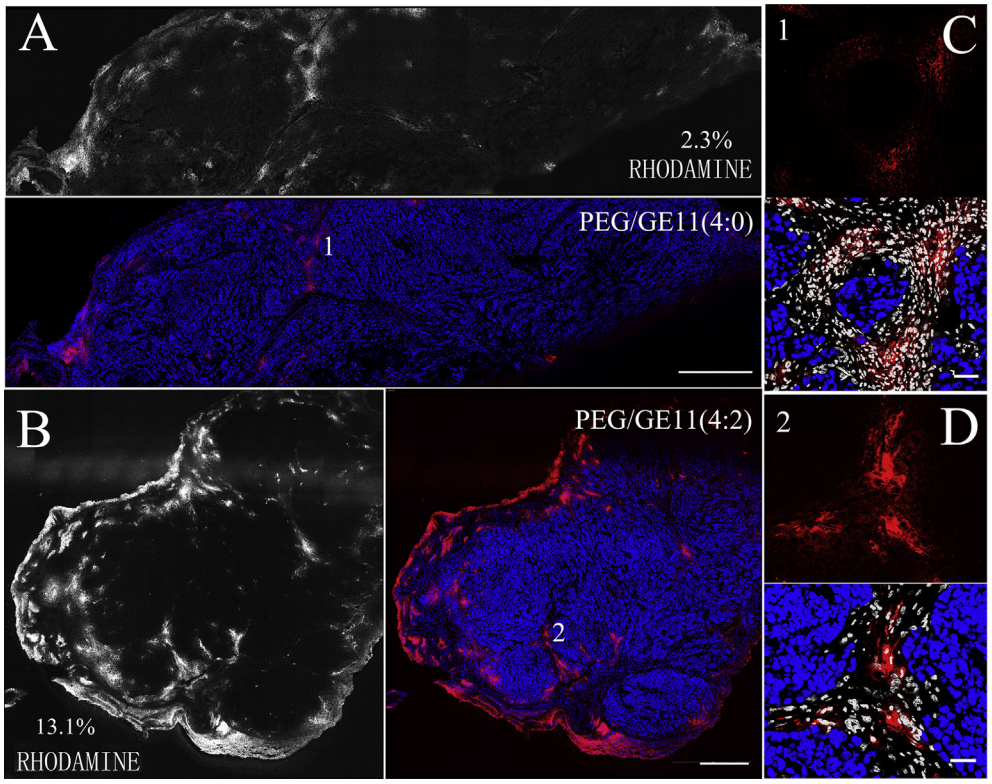

Figure 4 The overview image of the distribution of PLs (A) and GE11-TLs (B) in SMMC7721 xenografts after i.v. injection for 1 h. Scale bar: 440 μm. (C) and (D) The detailed drawing. Blue: nuclei; red: rhodamine-labeled liposomes; white: stromal cells. Scale bar: 50 μm.

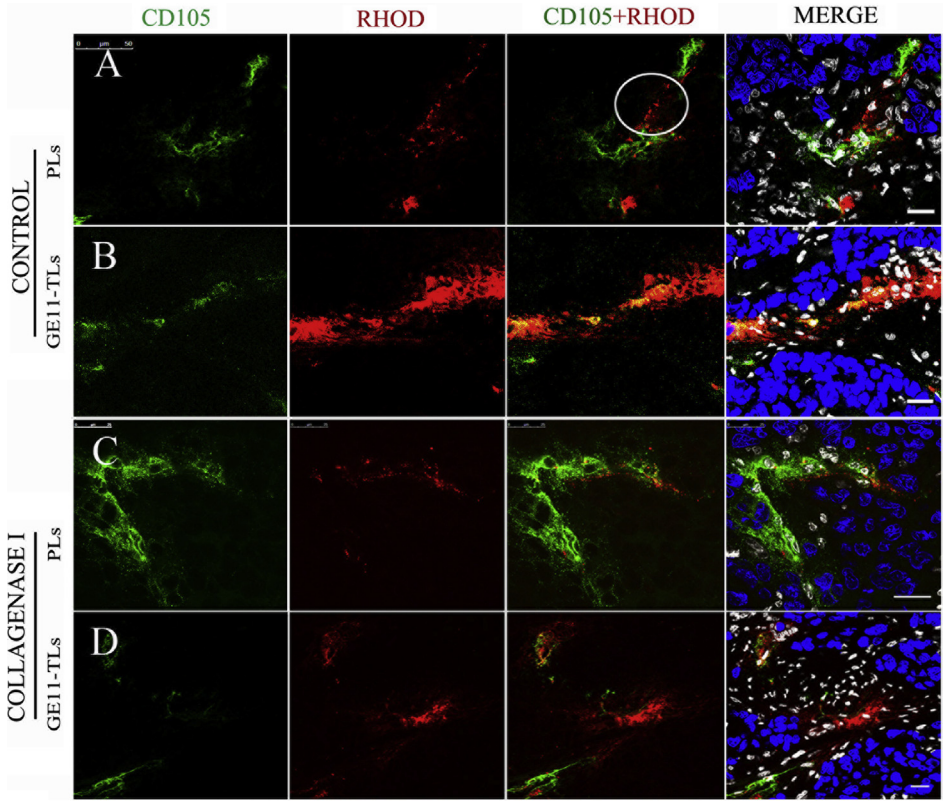

Figure 5 (A) and (B) The distribution of rhodamine-labeled GE11-TLs and PLs in the regions of tumor angiogenesis of SMMC7721 xenograft after i.v. injection for 1 h. (C) and (D) Images captured after i.v. injection of type I collagenase for 1 h. Blue: nuclei; green: tumor angiogenesis; red: rhodamine-labeled GE11-TLs or PLs; white: stromal cell. Scale bar: 20 μm.

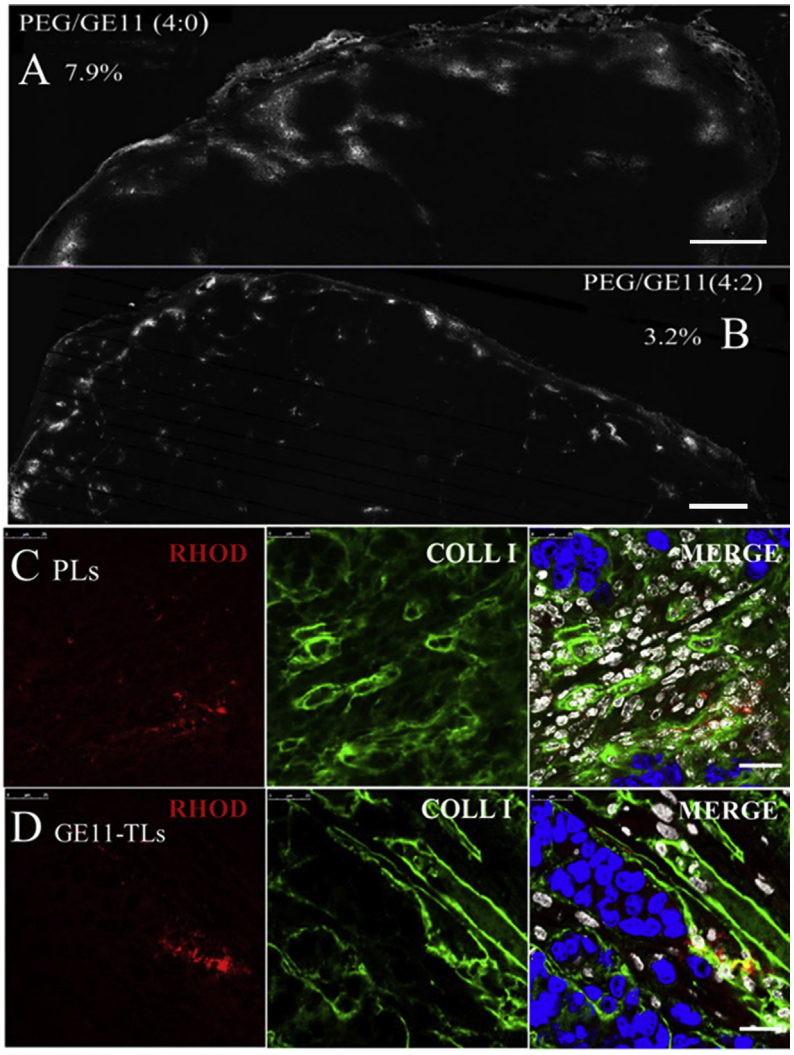

Figure 6 (A) and (B) The overview image of the distribution of rhodamine-labeled PLs and GE11-TLs in SMMC7721 xenograft after i.v. injection of type I collagenase for 1 h. Scale bar: 400 μm. (C) and (D) The distribution of rhodamine-labeled PLs and GE11 TLs in the SMMC7721 xenograft after i.v. injection of type I collagenase (30 mg/kg) for 1 h. Blue: nucleus; green: type I collagen; red: rhodamine-labeled liposome; white: stromal cell nucleus. Scale bar: 50 μm.

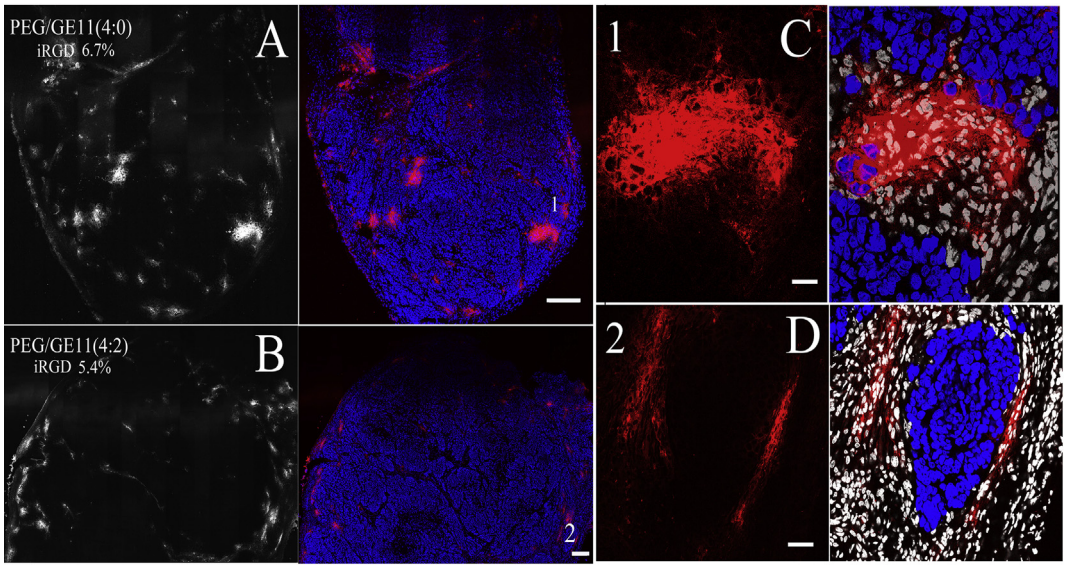

Figure 7 The distribution of rhodamine-labeled GE11-TLs and PLs in SMMC7721 xenograft combined with iRGD (16 mg/kg) after i.v. injection for 1 h. (A) and (B) Overview image. Scale bar: 200 μm; (C) and (D) Detail drawing. Scale bar: 25 μm. Blue: nucleus; red: rhodamine-labeled liposomes; white: stromal cell nuclei.

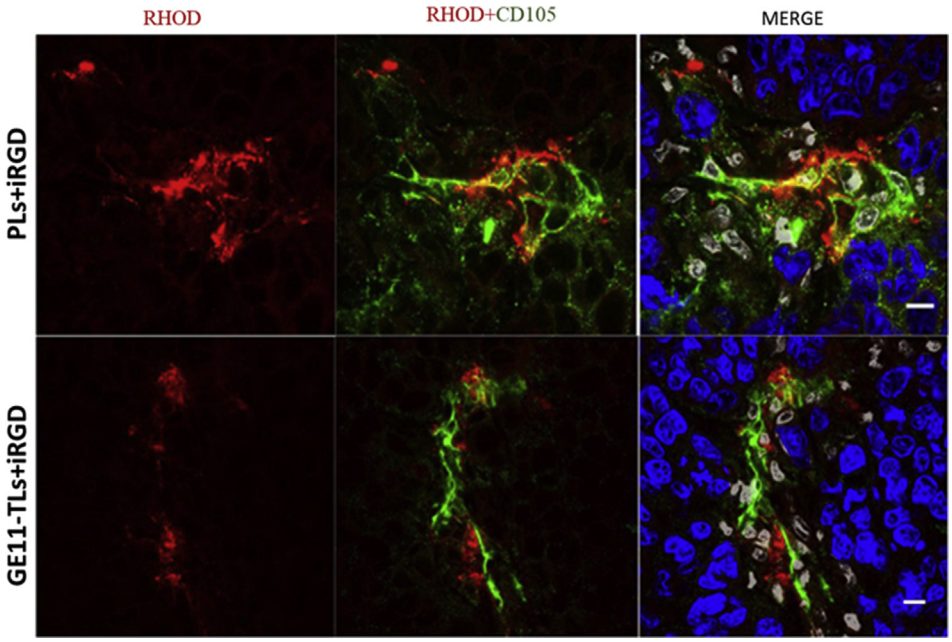

Figure 8 Distribution of rhodamine-labeled GE11-TLs [PEG/GE11 (4:2)] and PLs [PEG/GE11 (4:0)] in the regions of tumor neovascularization of SMMC7721 xenografts after i.v. combined with iRGD for 1 h, at the dose of 16 mg/kg. Scale bar: 10 μm. Blue: nucleus; red: rhodamine-labeled GE11-TLs or PLs; white: stromal cell nucleus.

case when IFP inside the tumor exceeds the microvascular fluid pressure. GE11 modification attenuates the intravasation of liposomes back to blood vessels. The binding-site barriers happened to GE11-modified liposomes also caused an embolization effect in the tumor angiogenesis region to exhibit better retention and accumulation in tumor site, comparing to passive-targeted liposomes. It is confirmed that GE11 peptide played a vital role in ligand-mediated EGFR-targeting transportation.

To overcome (some of) the delivery barriers mentioned above, alternative targeting strategies to endothelial cells have been

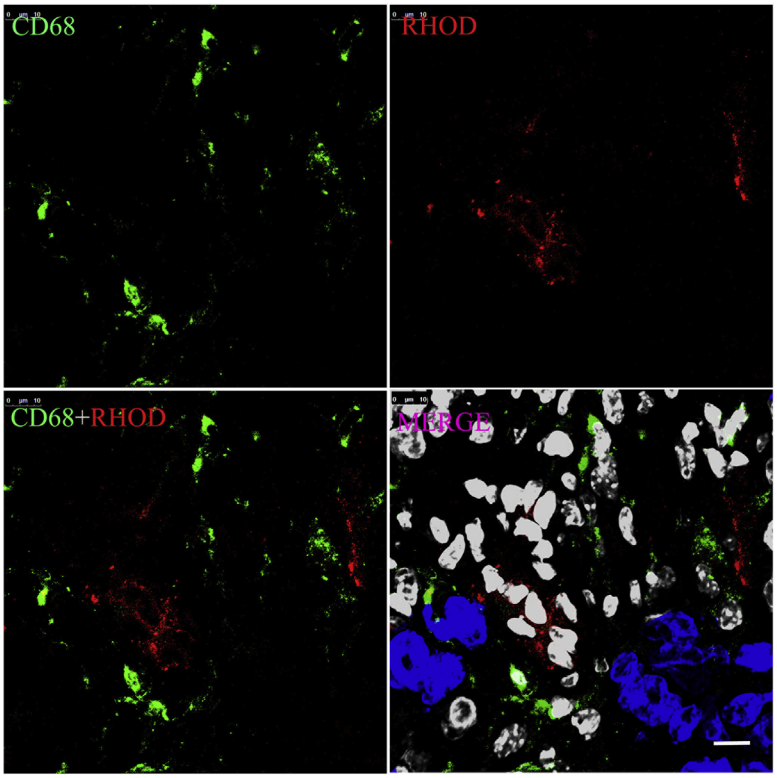

Figure 9 The phagocytosis behavior of macrophage in the SMMC7721 xenograft after i.v. co-injection of type I collagenase and rhodamine-labeled GE11-TLs for 1 h. Blue: nucleus; green: CD-68 labeled macrophage; red: rhodamine-labeled GE11-TLs; white: stromal cell nucleus. Scale bar: 25 μm.

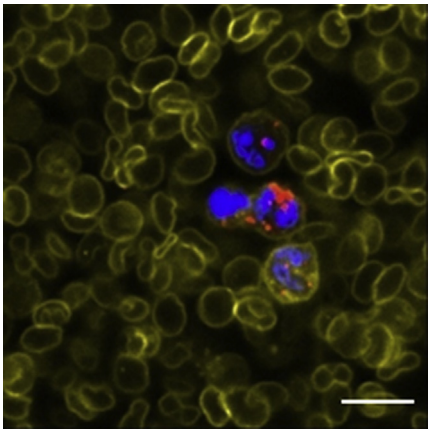

Figure 10 The phagocytose rates of mononuclear cells to GE11-TLs after i.v. injection for 12 h. Scale bar: 25 μm. Blue: nucleus; red: rhodamine-labeled GE11-TLs; yellow: WGA-labeled cell membrane.

designed and developed in current papers[33−35]. Interstitial cell targeting was also proposed in recent years, such as TAM and MDSC targeting[36−40].

4. Conclusions

In summary, we investigated the microenvironment of SMMC7721 xenograft, and also its interaction with GE11-TLs, an EGFR targeting liposome, to figure out the determinant obstacles for liposomes transport in tumor. EGFR positive interstitial cells in tumor microenvironment, rather than type I collagen fibers and filtrated macrophages, generated the pivotal barrier for deeper permeation for GE11-TLs. Collagenase I, which improved the accumulation and uptake of nanoparticles of PLs in previous study, had no impact on the distribution of GE11-TLs in SMMC7721 xenografts.

Acknowledgement

This work was supported by National Science Foundation of China (Grant Nos. 30825045 and 81273465).

Author contributions

Hailing Tang as first author and corresponding author was responsible for experiment design, data collecting, data processing, paper writing, paper submitting and revision. Mengjie Rui as second author was responsible for cell culture and animal experiment. Wei Guo as the third author was responsible for cell culture and tissue preparation. Junhua Mai was responsible for animal experiment, paper writing and revision. Yuhong xu is in charge of Hailing Tang's research work during her doctor's study.

Conflicts of interest

All the authors declare that there are no conflicts of interest.

Appendix A. Supporting information

Supporting data to this article can be found online at https://doi.org/10.1016/j.apsb.2019.06.011.

References

1. Sercombe L, Veerati T, Moheimani F, Wu SY, Sood AK, Hua S. Advances and challenges of liposome assisted drug delivery. *Front Pharmacol* 2015;**6**:286.
2. Allen TM, Cullis PR. Liposomal drug delivery systems: from concept to clinical applications. *Adv Drug Deliv Rev* 2013;**65**:36−48.
3. Barenholz Y. Doxil®—the first FDA-approved nano-drug: lessons learned. *J Control Release* 2012;**160**:117−34.
4. Tacar O, Sriamornsak P, Dass CR. Doxorubicin: an update on anticancer molecular action, toxicity and novel drug delivery systems. *J Pharm Pharmacol* 2013;**65**:157−70.
5. Passero Jr FC, Grapsa D, Syrigos KN, Saif MW. The safety and efficacy of Onivyde (irinotecan liposome injection) for the treatment of metastatic pancreatic cancer following gemcitabine-based therapy. *Expert Rev Anticancer Ther* 2016;**16**:697−703.
6. Beloqui A, Solinis MA, Rodriguez-Gascon A, Almeida AJ, Preat V. Nanostructured lipid carriers: promising drug delivery systems for future clinics. *Nanomedicine* 2016;**12**:143−61.
7. Naseri N, Valizadeh H, Zakeri-Milani P. Solid lipid nanoparticles and nanostructured lipid carriers: structure, preparation and application. *Adv Pharmaceut Bull* 2015;**5**:305−13.
8. Iyer AK, Khaled G, Fang J, Maeda H. Exploiting the enhanced permeability and retention effect for tumor targeting. *Drug Discov Today* 2006;**11**:812−8.
9. Kobayashi H, Watanabe R, Choyke PL. Improving conventional enhanced permeability and retention (EPR) effects; what is the appropriate target?. *Theranostics* 2013;**4**:81−9.
10. Owens 3rd DE, Peppas NA. Opsonization, biodistribution, and pharmacokinetics of polymeric nanoparticles. *Int J Pharm* 2006;**307**:93−102.
11. O'Neal SK, Lucas AT, Caron WP, Song G, Lay JC, Zamboni WC. Bidirectional interaction between nanoparticles and carrier-mediated agents and cells of the mononuclear phagocytic system. In: *Handbook of immunological properities of engineered nanomaterials. Engineered nanomaterials and the immune cell function*, vol. 3. World Scientific; 2016. p. 1−41.
12. García KP, Zarschler K, Barbaro L, Barreto JA, O'Malley W, Spiccia L, Stephan H, Graham B. Zwitterionic-coated "stealth" nanoparticles for biomedical applications: recent advances in countering biomolecular corona formation and uptake by the mononuclear phagocyte system. *Small* 2014;**10**:2516−29.
13. Blanco E, Shen H, Ferrari M. Principles of nanoparticle design for overcoming biological barriers to drug delivery. *Nat Biotechnol* 2015;**33**:941−51.
14. Salatin S, Maleki Dizaj S, Yari Khosroushahi A. Effect of the surface modification, size, and shape on cellular uptake of nanoparticles. *Cell Biol Int* 2015;**39**:881−90.
15. Jokerst JV, Lobovkina T, Zare RN, Gambhir SS. Nanoparticle PEGylation for imaging and therapy. *Nanomedicine* 2011;**6**:715−28.
16. Suk JS, Xu Q, Kim N, Hanes J, Ensign LM. PEGylation as a strategy for improving nanoparticle-based drug and gene delivery. *Adv Drug Deliv Rev* 2016;**99**:28−51.
17. Rodriguez PL, Harada T, Christian DA, Pantano DA, Tsai RK, Discher DE. Minimal "Self" peptides that inhibit phagocytic clearance and enhance delivery of nanoparticles. *Science* 2013;**339**:971−5.
18. Sosale NG, Spinler KR, Alvey C, Discher DE. Macrophage engulfment of a cell or nanoparticle is regulated by unavoidable opsonization, a species-specific "Marker of Self" CD47, and target physical properties. *Curr Opin Immunol* 2015;**35**:107−12.
19. Pattni BS, Chupin VV, Torchilin VP. New developments in liposomal drug delivery. *Chem Rev* 2015;**115**:10938−66.
20. Bunker A, Magarkar A, Viitala T. Rational design of liposomal drug delivery systems, a review: combined experimental and computational studies of lipid membranes, liposomes and their PEGylation. *Biochim Biophys Acta* 2016;**1858**:2334−52.

21. Fuchs BC, Hoshida Y, Fujii T, Wei L, Yamada S, Lauwers GY, et al. Epidermal growth factor receptor inhibition attenuates liver fibrosis and development of hepatocellular carcinoma. *Hepatology* 2014;**59**:1577−90.
22. Hopfner M, Sutter AP, Huether A, Schuppan D, Zeitz M, Scherubl H. Targeting the epidermal growth factor receptor by gefitinib for treatment of hepatocellular carcinoma. *J Hepatol* 2004;**41**:1008−16.
23. Song S, Liu D, Peng J, Sun Y, Li Z, Gu JR, Xu Y. Peptide ligand-mediated liposome distribution and targeting to EGFR expressing tumor *in vivo*. *Int J Pharm* 2008;**363**:155−61.
24. Li Z, Zhao R, Wu X, Sun Y, Yao M, Li J, et al. Identification and characterization of a novel peptide ligand of epidermal growth factor receptor for targeted delivery of therapeutics. *FASEB J* 2005;**19**:1978−85.
25. Tang H, Chen X, Rui M, Sun W, Chen J, Peng J, Xu Y. Effects of surface displayed targeting ligand GE11 on liposome distribution and extravasation in tumor. *Mol Pharm* 2014;**11**:3242−50.
26. Dolor A, Szoka Jr FC. Digesting a path forward: the utility of collagenase tumor treatment for improved drug delivery. *Mol Pharm* 2018;**15**:2069−83.
27. Khawar IA, Kim JH, Kuh HJ. Improving drug delivery to solid tumors: priming the tumor microenvironment. *J Control Release* 2015;**201**:78−89.
28. Eikenes L, Tari M, Tufto I, Bruland ØS, de Lange Davies C. Hyaluronidase induces a transcapillary pressure gradient and improves the distribution and uptake of liposomal doxorubicin (Caelyx™) in human osteosarcoma xenografts. *Br J Canc* 2005;**93**:81−8.
29. Cho HJ, Park SJ, Lee YS, Kim S. Theranostic iRGD peptide containing cisplatin prodrug: dual-cargo tumor penetration for improved imaging and therapy. *J Control Release* 2019;**300**:73−80.
30. Sugahara KN, Teesalu T, Karmali PP, Kotamraju VR, Agemy L, Greenwald DR, Ruoslahti E. Coadministration of a tumor-penetrating peptide enhances the efficacy of cancer drugs. *Science* 2010;**32**:1031−5.
31. Kandela I, Chou J, Chow K. Registered report: coadministration of a tumor-penetrating peptide enhances the efficacy of cancer drugs. *eLife* 2015;**4**:e06959.
32. Mantis C, Kandela I, Aird F. Replication study: coadministration of a tumor-penetrating peptide enhances the efficacy of cancer drugs. *eLife* 2017;**6**:e17584.
33. Zhao Y, Adjei AA. Targeting angiogenesis in cancer therapy: moving beyond vascular endothelial growth factor. *Oncol* 2015;**20**:660−73.
34. Wang J, Zhang L, Peng F, Shi X, Leong DT. Targeting endothelial cell junctions with negatively charged gold nanoparticles. *Chem Mater* 2018;**30**:3759−67.
35. Tietjen GT, Hosgood SA, DiRito J, Cui J, Deep D, Song E, et al. Nanoparticle targeting to the endothelium during normothermic machine perfusion of human kidneys. *Sci Transl Med* 2017;**9**:eaam6764.
36. Thomas SN, Schudel A. Overcoming transport barriers for interstitial-, lymphatic-, and lymph node-targeted drug delivery. *Curr Opin Chem Eng* 2015;**7**:65−74.
37. Qian Y, Qiao S, Dai Y, Xu G, Dai B, Lu L, Yu X, Luo Q, Zhang Z. Molecular-targeted immunotherapeutic strategy for melanoma *via* dual-targeting nanoparticles delivering small interfering RNA to tumor-associated macrophages. *ACS Nano* 2017;**11**:9536−49.
38. Singh Y, Pawar VK, Meher JG, Raval K, Kumar A, Shrivastava R, et al. Targeting tumor associated macrophages (TAMs) *via* nanocarriers. *J Control Release* 2017;**254**:92−106.
39. Kullberg M, Martinson H, Mann K, Anchordoquy TJ. Complement C3 mediated targeting of liposomes to granulocytic myeloid derived suppressor cells. *Nanomedicine* 2015;**11**:1355−63.
40. Saucedo AM, De La Cerda J, Suami H, Serda RE. Multimodal imaging of the tumor microenvironment and biological responses to immune therapy. *Biomed Microdevices* 2018;**20**:105.